Enhancing the Depth Resolution of Contactless Electrical Conductivity Imaging

Mehmet Nejat Tek, Bahram Shafai
Electrical and Computer Engineering Department
Northeastern University, Boston, MA
E-Mail: mtek@coe.neu.edu

***Abstract*— Contactless electrical conductivity imaging (CECI) collects magnetic field measurements of the induced currents from a biological subject. Because magnetic induction strength is highly dependent to the distance between the source and the measurements, information about the deeper conductivity variations are highly vulnerable to measurement noise. In this study, a novel form of the bounded data uncertainties (BDU) algorithm is designed to improve the depth resolution of CECI. The column weighted bounded data uncertainties (CWBDU) algorithm defines column-specific regularization parameters for ill-posed problems, such as CECI, without increasing the computational complexity of the problem. Performance of CWBDU is tested on a simulated CECI setup, and CWBDU results are presented with Tikhonov regularization, Moore Penrose inversion, and BDU results for comparison. The mean square error of the CWBDU images are at least 1.25 dB better than the mentioned algorithm results for all our test cases. In general, CWBDU seems to be promising tool for other ill-posed problems, such as electrical impedance tomography, and eddy current imaging.**

I. Introduction

The contactless electrical conductivity imaging (CECI) system employs a transducer that is composed of three coils, as illustrated in Fig. 1. Excitation coil, which resides on the center, is driven by low frequency AC currents. Detection coils are placed at the same distance to the excitation coil and wound in opposite directions. In the absence of any other objects, the cumulative voltage on the detection coils is calibrated to zero with nulling circuitry. In the vicinity of a conductive object, the excitation coil induces currents in the object, and detection coils measure a voltage that is dependent to the magnetic fields of the induction currents.

Earlier CECI studies proved that the data acquisition is possible while the induction currents are well within the safety limits of the biological tissues [1]. The physics behind the data acquisition system is simulated with finite element method (FEM) [2]. The simulations are used to reconstruct three dimensional conductivity images [3]. Finally, the data acquisition is realized, and images of actual physical phantoms are presented [4].

Due to the non-invasive nature of the CECI data acquisition, deeper portions of an object are further away from the transducers. Consequently, the excitation coil can produce weaker induction currents in deeper locations, and the magnetic fields of these currents are further weakened by the distance from the deeper location to the detection coils. In an imaging system, this fact makes information about deeper locations more vulnerable to measurement noise. The goal of this study is to mine as much information as possible while keeping the effects of the measurement noise under control.

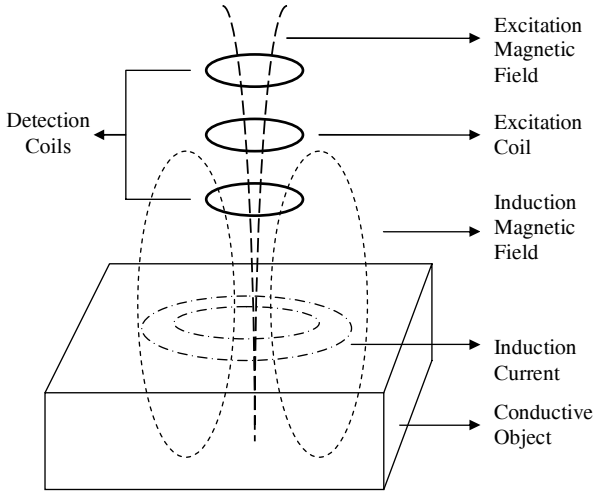

Fig. 1. General operation principle of a CECI transducer.

The next section presents a brief summary on the physics of the system. Then, image reconstruction algorithms are formulated for the CECI. The following section introduces a sample problem and numerical results. Conclusions and discussions are given in the final section.

II. Forward Problem

Forward problem aims to formulate the measurements in terms of the known physical parameters; transducer excitation and geometry, object geometry, and conductivity. For a typical CECI setup, the excitation coil carries low frequency (typically less than 100 kHz) sinusoidal currents and induce currents inside the conductive body. Induction currents have two sources: the primary magnetic vector potential $\vec{A}_p$ which originates from the excitation coil, and the scalar potential Φ, which is generated by the charge accumulation at the conductivity interfaces inside the body. The magnetic fields generated by the induction currents are expressed as [3]:

$$\vec{B}_i = -j\frac{\mu_0}{4\pi}\int \sigma(\omega\vec{A}_p + \nabla\phi) \times \frac{\vec{R}}{R^3} dV. \qquad (1)$$

The variables $\vec{B}_i$, ω, σ, and $\vec{R}$ represent the induction magnetic flux density, the radial frequency, conductivity distribution, and the displacement vector that points from the source to the measurement point, respectively.

Due to conductivity dependence of Φ, (1) reveals the nonlinear relation between the conductivity and the measurements. Nevertheless, it is possible to approximate a linear relation around an assumed conductivity distribution σ_0. For this distribution, the measurements $\vec{B_{i0}}$ can be calculated. Afterwards, an arbitrary conductivity distribution can be expressed as $\sigma = \sigma_0 + \Delta\sigma$, and measurement perturbations $\Delta\vec{B}_i$ can be related to the conductivity perturbations [3]

$$\Delta\vec{B}_i = j\frac{\mu_0}{4\pi}\int \frac{\vec{R}}{R^3} \times \left(\omega\vec{A}_p + \nabla\phi_0 + \frac{\partial(\nabla\phi)}{\partial\sigma}\right)\Delta\sigma \; dV_{\text{body}}. \tag{2}$$

For a digitized implementation, the conductive body is divided into homogeneous voxels and scalar potential Φ_0 is numerically calculated with FEM [5]. The discrete form of (2) is a linear set of equations

$$Sx = b \tag{3}$$

where x is the unknown conductivity perturbations vector, b is the magnetic field measurements vector, and S is the sensitivity matrix.

III. Inverse Problem

The inverse problem is concerned with reconstructing images: given the transducer geometry, excitation, and measurements, inverse problem aims to estimate the spatial conductivity distribution of the object. In this study, the inverse problem focuses on deriving an inverse relation to (3). In an imaging scenario, one has to account for the noise y that is inherently embedded into the measurements; $y = Sx - b$. Then, the least squares estimation problem of solving x is given as

$$\min_x \|Sx - b\|^2. \tag{4}$$

Note that $\|.\|$ represents the Euclidean norm for vectors, and maximum singular value for the matrices. The solution of the least squares problem is

$$\hat{x} = (S^T S)^{-1} S^T b. \tag{5}$$

However, the least squares solution may not be acceptable for the ill-posed problems. Measurement noise may be easily amplified in the least squares solution, and render the results useless. To control this behavior, four algorithms are adopted to the CECI inverse problem in this study.

A. Tikhonov Regularization

Tikhonov's idea is to incorporate another term to the least squares problem that limits the norm of the solution

$$\min_x(\|Sx - b\|^2 + \alpha\|x\|^2) \tag{6}$$

leading to regularization

$$\hat{x} = (S^T S + \alpha I)^{-1} S^T b. \tag{7}$$

Although there are cases where the ad-hoc α values are feasible, the image quality is usually sensitive to α: a low α may not suppress the effects the measurement noise properly, and a high α may lead to unnecessary information loss. An optimal α is determined according to the generalized cross validation (GCV) criterion as [6]

$$\min_\alpha \frac{||(I - S(S^T S + \alpha I)^{-1} S^T)b||^2}{\text{Trace}[I - S(S^T S + \alpha I)^{-1} S^T]^2}. \tag{8}$$

B. Moore Penrose Inversion

Moore Penrose inversion (MPI) algorithm is based on the singular value decomposition of the sensitivity matrix S

$$\begin{aligned} U &= [u_1, \ldots, u_m] \\ V &= [v_1, \ldots, v_n] \\ U^T S V &= \Sigma = \text{diag}(\sigma_1, \ldots, \sigma_q), \quad q = \min(m, n). \end{aligned} \tag{9}$$

The σ_i are the singular values of the matrix S in descending order, i.e. $\sigma_1 \geq \sigma_2 \geq \ldots \geq \sigma_q \geq 0$. A minimum norm least squares solution of the system is given as

$$\hat{x} = \sum_{i=1}^{p} \frac{1}{\sigma_i} u_i^T (b + y) v_i \tag{10}$$

Ideally the upper limit of the summation is equal to the rank of the matrix, i.e. $p = q$. However, the noise term in (10) may dominate the solution for an ill-posed matrix, if the summation is not terminated earlier. Optimal truncation index is the maximum p that satisfies [7]

$$20\log\frac{\sigma_1}{\sigma_p} \leq \text{SNR} \tag{11}$$

$$\text{SNR} = 10\log\frac{E(\|b\|^2)}{E(\|y\|^2)} \tag{12}$$

where $E(.)$ is the expected value operator. Truncating singular vectors keeps the effects of the noise under control. However, the information carried by the truncated singular vectors is lost as well.

C. Bounded Data Uncertainties

Developed in the robust control context, bounded data uncertainties (BDU) analyzes the problem on a more detailed mathematical model. The problem is expressed as

$$y = (S + \Delta S)x - (b + \Delta b) \tag{13}$$

where ΔS and Δb are the uncertainties in the matrix and, in the measurement vector, respectively. The upper limits for these uncertainties are assumed to be available, $\|\Delta S\| \leq \eta$, and $\|\Delta b\| \leq \eta_b$. Using the upper limits, BDU formulates the least squares problem to minimize the maximum possible residual norm [8]

$$\min_x(\|Sx - b\| + \eta\|x\| + \eta_b). \tag{14}$$

The minimization process reduces the problem into two equations; (7) coupled with

$$\alpha = \eta\frac{\|S\hat{x} - b\|}{\|\hat{x}\|}. \tag{15}$$

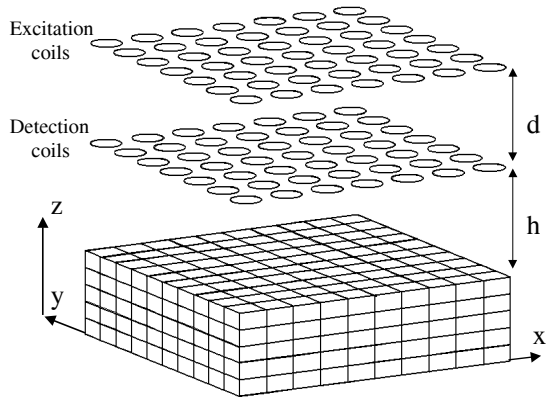

Fig. 2. Sample problem setup for image reconstruction. Depth is defined as the distance from the detection coils plane. h=d=0.5cm is used for the simulations. Note that, h and d are exaggerated to ease display.

The coupled equations can be solved with SVD techniques as described in [8].

D. Column Weighted Bounded Data Uncertainties

We introduce a weighted variant of the BDU algorithm (CWBDU) that can flexibly scale the regularization parameter along the columns of the sensitivity matrix. The least squares problem is altered into

$$\min_x(\|Sx-b\|+\eta\frac{\|S\|\|x\|^2}{\|b\|}+\eta_b). \tag{16}$$

Notice that the second term is weighted by $\|S\|\|x\|/\|b\|$ which is expected to be close to unity. This is specifically designed not to alter the least squares problem from the original BDU formulation.

The advantage of the weighted form is that it provides the foundation to base the scaled regularization. Without the loss of generality, let us assume that S is partitioned into two sub-matrices $S_1(m\times n_1)$ and $S_2(m\times n_2)$, and the uncertainty bounds for each sub-matrix is available, i.e. $\|\Delta S_1\|\le\eta_1$ and $\|\Delta S_2\|\le\eta_2$. The solution of the least squares problem is

$$\hat{x} = (S^TS+\alpha D)^{-1}S^Tb \tag{17}$$

$$D = \begin{bmatrix} \eta_1\|S_1\|I_{n_1} & \\ & \eta_2\|S_2\|I_{n_2} \end{bmatrix} \tag{18}$$

$$\alpha = \frac{\|S\hat{x}-b\|}{\|b\|}. \tag{19}$$

These formulae prove that it is possible to apply different regularization to each column without increasing the search space for the parameter α, provided that uncertainty limits for each column are available.

IV. Results

The sample test setup in [3] is used as a comparison basis for the mentioned algorithms. In this setup, a conductive body of 10 cm×10 cm×5 cm is comprised of 1 cm×1 cm× 1 cm voxels for image reconstruction. A 7×7 array of transducers are placed at a plane 0.5 cm above the surface of the conductive object. Each transducer has 3 coils with radii 0.5 cm, and the detection coils are 0.5 cm away from the excitation coil. Transducer centers are 1.5 cm away from the neighboring transducers. The setup is shown in Fig. 2.

TABLE I

Mean square error of the vertical line image reconstructions for different measurement noise levels.

SNR(dB)	MSE(dB) MPI	Tikhonov	BDU	CWBDU
20	-0.86	-1.50	-1.39	-2.68
30	-1.29	-2.11	-1.90	-3.33
40	-1.48	-2.80	-2.52	-4.02
50	-1.68	-3.44	-3.15	-4.86
60	-2.68	-4.03	-3.79	-5.70

For one experiment, one transducer is driven at 50 kHz, and the magnetic field is measured with all 49 transducers. The experiment is repeated for all excitation coils, accumulating 2401 (49×49) measurements for the 500 unknown voxel conductivities. The matrix $S(2401\times500)$ is simulated assuming a uniform conductivity distribution of 0.02 S/m, and perturbations from this distribution are being imaged. For a certain phantom, the measurement vector is calculated with (2), and white Gaussian noise is added to the measurements.

The singular value analysis revealed that the condition number of the matrix S is 7.41×10^6. Due to the high condition number, the SNR of the data acquisition system can degrade the inverse problem results easily. The high condition number is the result of a large survey depth (distance to the detection coils in z axis) in the object. For every 1 cm depth increase, the measured signal decreases by approximately 14 dB. Consequently, it is a challenge to image deeper voxel perturbations in the presence of surface voxel perturbations. To explore this phenomenon, vertical line image is selected as the test phantom.

BDU and CWBDU algorithms require upper limits for the uncertainties at various different measurement noise levels. Measurement noise disappears from equations (15) and (19). However, the measurement noise has a projection onto the matrix uncertainty space, and this projection may dominate the matrix uncertainty norm if the measurement noise norm is much greater than the uncertainty norm. The uncertainty matrix norm of this problem is modeled as

$$\|\delta S\|\le\eta = (10^{-5}+10^{-2-\frac{SNR}{20}})\|S\|$$
$$\|\delta S_i\|\le\eta_i = (10^{-3}+10^{-\frac{SNR}{20}})\|S\|,\quad i=1,...,500.$$

This noise model is merely an approximation that assumes that about %1 of the measurement noise norm can effectively be treated as sensitivity matrix uncertainty.

The MSE of the reconstructions are given in Table I. Note that mean squared error (MSE) is defined as

$$\text{MSE}=10\log\frac{E(\|x-\hat{x}\|^2)}{E(\|x\|^2)}. \tag{20}$$

Reconstructions with the CWBDU and Tikhonov's algorithm are shown in Figures 3-6, respectively.

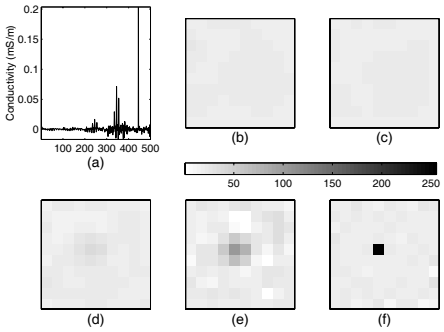

Fig. 3. The vertical line image reconstructed using Tikhonov regularization when measurement SNR is set to 20 dB. The conductivity profile is shown in (a) where horizontal axis is the voxel index. Voxels are numbered such that indices 1-100 are at 5cm depth, 101-200 are in 4 cm depth, and so on. The image at 5cm, 4cm, 3cm, 2cm, and, 1cm depths are shown in (b), (c), (d), (e), and, (f) respectively.

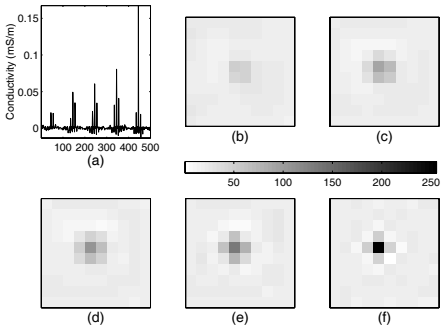

Fig. 4. The vertical line image reconstructed using CWBDU when measurement SNR is set to 20 dB. The conductivity profile is shown in (a) where horizontal axis is the voxel index. Voxels are numbered such that indices 1-100 are at 5cm depth, 101-200 are in 4 cm depth, and so on. The image at 5cm, 4cm, 3cm, 2cm, and, 1cm depths are shown in (b), (c), (d), (e), and, (f) respectively.

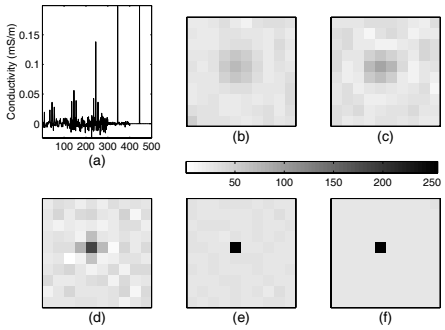

Fig. 5. The vertical line image reconstructed using Tikhonov regularization when measurement SNR is set to 60 dB. The conductivity profile is shown in (a) where horizontal axis is the voxel index. Voxels are numbered such that indices 1-100 are at 5cm depth, 101-200 are in 4 cm depth, and so on. The image at 5cm, 4cm, 3cm, 2cm, and, 1cm depths are shown in (b), (c), (d), (e), and, (f) respectively.

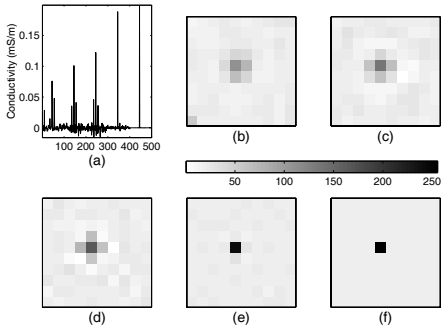

Fig. 6. The vertical line image reconstructed using CWBDU when measurement SNR is set to 60 dB. The conductivity profile is shown in (a) where horizontal axis is the voxel index. Voxels are numbered such that indices 1-100 are at 5cm depth, 101-200 are in 4 cm depth, and so on. The image at 5cm, 4cm, 3cm, 2cm, and, 1cm depths are shown in (b), (c), (d), (e), and, (f) respectively.

V. Conclusions and Discussions

A weighted form of BDU algorithm is introduced to achieve column specific regularization for ill-posed problems. The formulation is tested on the CECI inverse problem, and results are compared to well-known least squares algorithms. CWBDU algorithm results have at least 1.25 dB less MSE compared to all other algorithms for the test case. Furthermore, it is possible obtain minor improvements in the CWBDU reconstructions by fine tuning the uncertainty norm η.

In an unsupervised environment, the uncertainty norm estimate needs to have a reasonable error margin. In order to evaluate the effect of uncertainty bound errors, the uncertainty bound η is altered $\pm 50\%$ from (20), and MSE increases are found to be less than 0.1dB. This fact confirms the robustness of the algorithm, and suggests that the algorithm results will be statistically stable.

The depth resolution of the CECI system is found to be highly dependent to the measurement SNR. With the new algorithm, the CECI system is capable of providing low resolution images at 3 cm depth with 20 dB SNR.

References

[1] N. G. Gencer and M. N. Tek, "Imaging Tissue Conductivity via Contactless Measurements: A Feasibility Study", *Elektrik, Turkish J. of Electrical Eng. & Computer Science*, Vol. 6, pp. 183-200, 1998.

[2] N. G. Gencer and M. N. Tek, "Forward Problem Solution for Electrical Conductivity Imaging via Contactless Measurements", *IOP Physics in Medicine and Biology*, Vol. 44, pp. 927-940, April 1999.

[3] N. G. Gencer and M. N. Tek, "Electrical Conductivity Imaging via Contactless Measurements", *IEEE Tran on Medical Imag.*, Vol. 18, pp. 617-627, July 1999.

[4] B. U. Karbeyaz, N. G. Gencer, "Electrical Conductivity Imaging via Contactless Measurements: An Experimental Study", *IEEE Tran on Medical Imag.*, Vol. 22, pp. 627-625, May 2003.

[5] M. N. Tek and N. G. Gencer, "A New 3D FEM formulation for the Solution of Potential Fields in Magnetic Induction Problems", *Proc. of the 19th Annual Int. Conf. of the IEEE-EMBS*, pp. 2470-2473, Chicago, 1997.

[6] G. H. Golub and M. Heath, "Generalized cross-validation as a method for choosing a good ridge parameter", *Technometrics*, Vol. 21, No. 2, pp. 195-197, May 1979.

[7] Y. S. Shim and Z. H. Cho, "SVD pseduo-inversion Image Reconstruction", *IEEE Tran on Ac. Speech and Signal Proc.*, Vol. ASSP-29, pp. 904-909, 1981.

[8] S. Chandrasekaran, G. H. Golub, M. Gu, and, A. H. Sayed, "Parameter estimation in the presence of bounded data uncertainties", *SIAM J. Matrix Anal. Appl.*, Vol. 19, No. 1, pp. 235-252, Jan 1998.